Periodica Polytechnica Electrical Engineering and Computer Science, 70(1), pp. 104–111, 2026

Synthesizing Shaped Beams with Prescribed Footprint Illumination for Specific Coverage Applications

Jafar Ramadhan Mohammed[1]*

[1] College of Electronic Engineering, Ninevah University, Al-Majmoaa Street, 41002 Mosul, Iraq
* Corresponding author, e-mail: jafar.mohammed@uoninevah.edu.iq

Received: 29 December 2025, Accepted: 11 June 2026, Published online: 24 June 2026

Abstract

In many wireless personal communication applications such as medical microwave imaging, geostationary satellite, radar, and unmanned aerial vehicle communications, the shape of the radiated beam by an antenna array must be precisely matched to the required coverage area on the intended object to achieve maximum performance. In this paper, an iterative fast Fourier transform (IFFT) method is adopted for producing arbitrary targeted footprint patterns. The IFFT method exploits Fourier transform relationships to iteratively transform between array excitation weights and far-field radiation patterns, enabling fast and effective synthesis of complex shaped-beam footprints compared to all other optimization algorithms. For medical microwave imaging applications three different targeted footprints of triangular, square, and circular shapes are considered as samples, while for geostationary satellite applications, a complex footprint of Iraq-Map outline is considered. Simulation results have proved the effectiveness of the proposed method for efficiently generating the required footprints without the need for heavy optimization solvers. Moreover, some complicated coverage shapes such as the geographical outline of Iraq, require more degrees of freedom in the antenna array design, which increases both the cost and the array complexity. To solve this problem, a thinning method was used to remove array elements that have only a small influence on the overall radiation pattern.

Keywords

planar arrays, array pattern synthesis, iterative FFT, prescribed footprint illuminations

1 Introduction

A sensor array is a collection of microphones, acoustic transducers, or antennas arranged in a certain geometry pattern such as linear, rectangular, circular, or even randomly. Its far-field radiation pattern can be synthesized to approach a required beam shape. Thus, it is widely used for geostationary satellite applications [1], health monitoring systems [2, 3], radar [4], unmanned aerial vehicle communications [5], and many other applications. To deliver maximum power, the shape of the radiated power patterns must be precisely coincident to the shape of the required coverage areas on the intended objects or Earth's region. The required array radiation patterns should be synthesized with a relatively small number of radiating elements to keep the array cost and complexity as small as possible. The far-field radiation patterns can be properly shaped according to the prescribed footprints by controlling the feeding amplitudes and phases of the array elements. This problem has received much attention in recent years [5–10]. The control of inter-element spacing was also used for shaping the array radiation patterns [11, 12]. For fixed array geometry where the inter-element spacing and element positions are all fixed, thus, the only unknown design parameters are elements' excitations (it could be in terms of amplitude-only control, phase-only control, or even both the amplitude and phase control). The problem of optimizing elements' excitations has been solved in a globally-optimal fashion using different optimization algorithms such as genetic algorithm [13–15], particle swarm optimization [16, 17], convex optimization [18–20], and even deep learning algorithms [21]. However, all of these global optimization algorithms are complex and they are time consuming especially when dealing with complex footprint shapes that require a large number of array elements. Other methods are based on a modified Woodward-Lawson method [22] and the superposition principle [23]. On the other hand, the iterative FFT method has proved its

Cite this article as: Mohammed, J. R. "Synthesizing Shaped Beams with Prescribed Footprint Illumination for Specific Coverage Applications", Periodica Polytechnica Electrical Engineering and Computer Science, 70(1), pp. 104–111, 2026. https://doi.org/10.3311/PPee.43214

capability of synthesizing array patterns with fast convergence time and quite simplicity [24–27]. In this paper, the iterative FFT method was adopted to design planar arrays with arbitrary far-field radiation footprints and quite complex shapes. The shape of the targeted radiation footprint patterns should be conformed to the shape of the coverage area on Earth/object. In satellite and unmanned aerial vehicle applications, the coverage region on the Earth is relatively flexible, while for medical microwave imaging applications, the coverage area on the objects is limited and it should be more precise and accurate especially in medical treatments by microwave radiations. The presented IFFT method improves microwave imaging performance and at the same time it reduces the system cost and complexity, making it a practical solution for real-world biomedical imaging applications.

2 Mathematical models and problem formulation

Consider a two-dimensional rectangular array of $N \times M$ isotropic radiator elements spaced along x-axis and y-axis by dx and dy, respectively. The complex element excitation weights (i.e., in terms of both amplitude and phase) of any elements can be represented by $w_{n,m} e^{j\varnothing_{n,m}}$. The overall far-field array factor that radiated by such planar array can be written as:

$$AF(u,v) = \sum_{n=1}^{N} \sum_{m=1}^{M} w_{n,m} \; e^{jk\left[nd_x u + md_y v\right]}, \tag{1}$$

where $w_{n,m} = a_{n,m} e^{j\varnothing_{n,m}}$ is the amplitude and phase excitations of the array elements, $k = 2\pi/\lambda$ is the wave number, λ is the wave length, $u = \sin\theta\cos\varphi$, $v = \sin\theta\sin\varphi$, θ and φ are the elevation and azimuth angles, respectively.

For simplicity, we assume a unit element pattern, and then the total radiation pattern magnitude is same as that of the array factor:

$$FP(u,v) = \left|AF(u,v)\right|. \tag{2}$$

Let $FP(u, v)$ be the target footprint where it is equal to unity inside the footprint shape and a small value outside the shape. For example, if we want a footprint pattern like a shape of circular, triangular, rectangular, Iraq outline map, or any other arbitrary shape), then the radiated array factor of the planar array should be approximately equal to the targeted footprint shape:

$$AF(u,v) \approx FP(u,v). \tag{3}$$

From Eq. (1), it is clear that the only design parameters are $w_{n,m}$, d_x and d_y. For uniformly spaced planar arrays, we fix the inter-element spacing at $d_x = d_y = 0.5\ \lambda$. Thus, the only element excitation amplitudes, $a_{n,m}$, and phases, $\varnothing_{n,m}$, are the design variables and the problem can be formulated as:

- Find $a_{n,m}$, and for $n = 1, \dots N$ and $m = 1, \dots M$ such that the $AF(u, v)$ best matches the $FP(u, v)$ according to Eq. (3).

3 The iterative FFT method

The design problem that was presented in Eq. (3) can't be solved as a simple linear problem due to many target constraints. The iterative FFT method can perform very well with this problem because premirly depends on the existence relationship between array factor and the element excitations through direct and inverse Fourier transform. In other words, the iterative FFT projects back and forth between element excitations and array factor under some desired constraints until the radiated pattern of the array factor best matches the targeted footprint shape with minimized sidelobe level in an iterative manner.

The proposed iterative FFT method consists of the following procedures:

1. Start with initial weights of amplitudes and phases. For example, unit amplitudes and zero phases.
2. Compute the $AF(u, v)$ at iteration i using the initial weights, as follows:
   - $AF^i(u, v) = \mathscr{F}\{w^i\}(u, v)$ where $\mathscr{F}$ is the Fourier transform operator according to Eq. (1).
3. Replace its magnitude by the magnitude of the targeted footprint:
   $$AF^i_{\text{new}}(u,v) = FP^i(u,v)\frac{AF^i(u,v)}{\left|AF^i(u,v)\right|}.$$
4. Transform $AF^i_{\text{new}}(u,v)$ back to the corresponding element excitation weights:
   $$w^i_{\text{new}} = \mathscr{F}^{-1}\left\{AF^i_{\text{new}}(u,v)\right\}.$$
5. Apply constraints such as thinning elements as follows:
   - $w^{i+1} = w^i_{\text{new}} \cdot \text{Thinning}$ where Thinning is equal to 1 for active or ON elements and 0 for inactive or OFF elements. Other constraints on the element excitations such as the required dynamic range ratio may be also included in this step.
6. Repeat the above steps until the resultant array pattern matches the target footprint shape within an acceptable tolerance or the method reached the maximum number of iterations.

That is, the method convergence when:

$$\left\| \left| AF^{i}(u,v) \right| - FP(u,v) \right\| \rightarrow 0.$$

In this paper, it is considered four different targeted footprint shapes like circular, rectangular, triangular, and Iraq outline. These footprints are as follows:

$$FP_{\text{circular}}(u,v) = \begin{cases} 1, & \sqrt{u^2+v^2} \leq r_o \\ \varepsilon, & \text{otherwise} \end{cases}, \tag{4}$$

$$FP_{\text{rectangular}}(u,v) = \begin{cases} 1, |u| \leq u_o, |v| \leq v_o \\ \varepsilon, \quad \text{otherwise} \end{cases}. \tag{5}$$

For triangular footprint, it can be defined by inequality of a triangular shape in (u, v) plane, while for Iraq footprint outline; it is derived from a binary image of Iraq map. Nevertheless, any other shapes can be accurately synthesized by the proposed method. Generally, for synthesizing complex shapes such as Iraq map outline, larger planar arrays may be needed to provide sufficient number of degrees of freedom and a thinning process may be applied to remove some weak elements that have negligible effect on the formed radiation pattern. The value of ε which is outside the footprint region is chosen to be small $\varepsilon = 10^{-3}$ to get suppressed sidelobe level. Note that when substituting any of these targeted footprints in step 3 above and iteratively drives new array factor patterns, their sidelobe patterns that are outside the targeted footprints will be minimized according to the constraint value of $\varepsilon = 10^{-3}$. It should be also mentioned that the minimum achievable sidelobe levels depend directly on the number of array elements. In another words, greater number of degrees of freedom will result in better sidelobe suppression. However, as mentioned this will dramatically increase the array cost and complexity. Therefore, we suggest a thinning method to efficiently remove only the weak elements whose amplitude excitations are smaller than a specific threshold (for example, a small threshold value of 0.01) in which their effects on the resulting radiation pattern are negligible. Thus, the number of the active elements that need RF components can be greatly reduced while still maintaining the array performance unchanged. The element excitations with this thinning process can be written as:

$$w'_{nm} = \begin{cases} w_{nm}, & w_{nm} \geq \text{threshold} \\ 0 & w_{nm} < \text{threshold} \end{cases}. \tag{6}$$

Here threshold represents the minimum value of the element excitations in the designed array. Note that the amplitude excitations are normalized to one, thus the maximum value is equal to one. The dynamic range ration (DRR) can be defined as the ratios between maximum and minimum values of the amplitude excitations. For unit-amplitudes uniform array, this value is equal to one which is the best value. Larger values indicate higher complexity in the feeding network. If we choose threshold = 0.1 instead of 0.01, then the DRR will be reduced from 100 to only 10 while the percentage of weak elements removal will be also higher at the cost of higher undesirable sidelobe levels in the synthesized radiation pattern.

4 Simulation results

In all examples, the radiating system has been set as an equal-spaced planar array composed by a different number of elements along the x- and y-axes. Different far-field radiation footprints such as triangular, square, circular, Iraq land footprints have been synthesized and evaluated as follows in Sections 4.1 to 4.4.

4.1 Triangular footprint shape

The number of the considered planar array elements was $N \times M = 48 \times 64$. The shape of the targeted triangular footprint is shown in Fig. 1 (a), while the shape of the synthesized triangular footprint is shown in Fig. 1 (b). The three-dimension and two-dimensional plots of the obtained far-field radiation patterns are shown in Fig. 2. From Fig. 2, it can be seen that the required far-field radiation

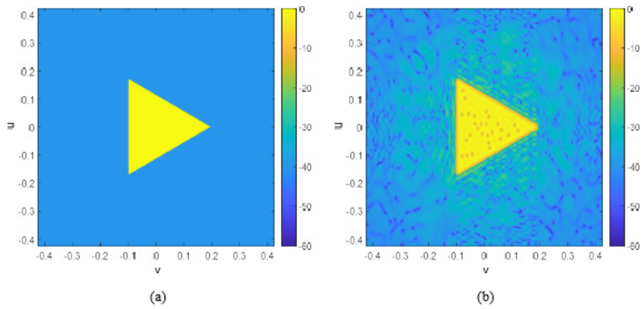

Fig. 1 The results of triangular footprint: (a) Desired shape; (b) Synthesized shape

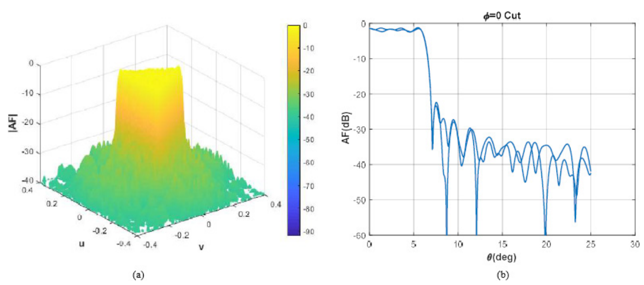

Fig. 2 The triangular footprint radiation patterns: (a) 3D pattern; (b) 2D pattern

footprint has been precisely synthesized and the peak sidelobe level of the radiated power outside the boundary of footprint shape has been reduced to more than −22.57 dB. The corresponding amplitude and phase excitations of the designed planar array are shown in Fig. 3.

4.2 Square footprint shape

In this case, the number of the planar array elements was also $N \times M = 48 \times 64$. The shape of the desired square footprint is shown in Fig. 4 (a), while the shape of the synthesized square footprint is shown in Fig. 4 (b). The three-dimension and two-dimensional plots of the obtained far-field radiation patterns are shown in Fig. 5. For this footprint, also observe that the required far-field radiation footprint has been precisely met and the peak sidelobe level was at −20.0 dB. The corresponding amplitude and phase excitations of the designed planar array are shown in Fig. 6.

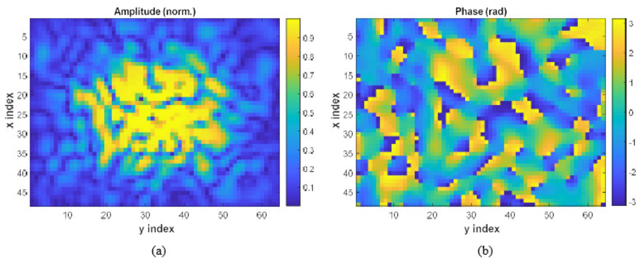

Fig. 3 The synthesized triangular footprint: (a) Amplitude excitations; (b) Phase excitations

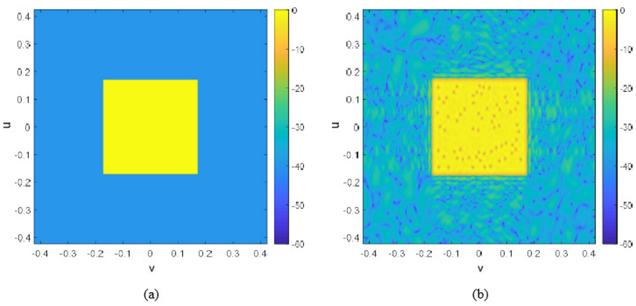

Fig. 4 The results of square footprint: (a) Desired shape; (b) Synthesized shape

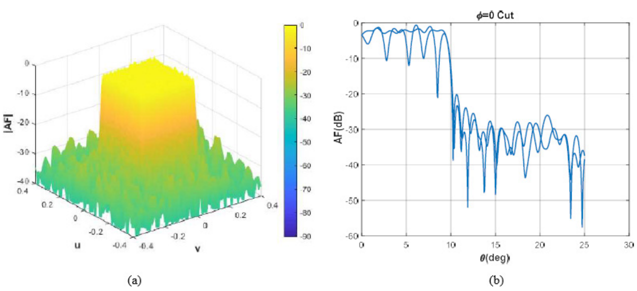

Fig. 5 The square footprint radiation patterns: (a) 3D pattern; (b) 2D pattern

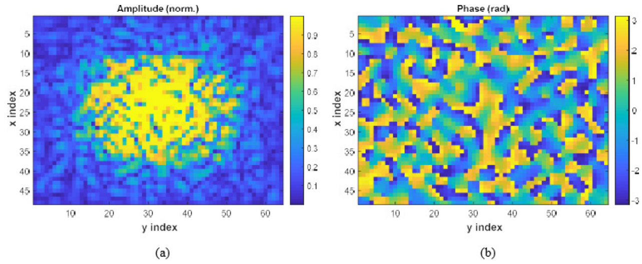

Fig. 6 The synthesized square footprint: (a) Amplitude excitations; (b) Phase excitations

4.3 Circular footprint shape

In this scenario, the same planar array elements $N \times M = 48 \times 64$ was used. The shape of the targeted circular footprint is shown in Fig. 7 (a), while the shape of the synthesized circular footprint is shown in Fig. 7 (b). The three-dimension plot of the obtained far-field radiation pattern is shown in Fig. 8. From Fig. 8, it can be seen that the required far-field radiation footprint has been precisely met and the peak sidelobe level of the radiated power outside the required footprint has been reduced to more than −20.7 dB.

Also, it is noted some high ripples in the flat-top region of the main beam pattern. The corresponding amplitude and phase excitations of the design planar array are shown in Fig. 9.

4.4 Iraq land footprint

In this case, the number of the planar array elements was increased to $N \times M = 100 \times 100$ to provide sufficient

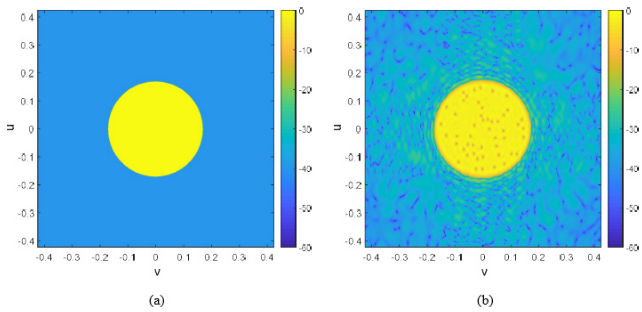

Fig. 7 The results of circular footprint: (a) Desired shape; (b) Synthesized shape

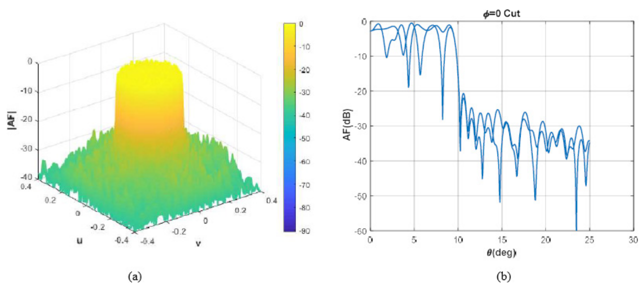

Fig. 8 The circular footprint radiation patterns: (a) 3D pattern; (b) 2D pattern

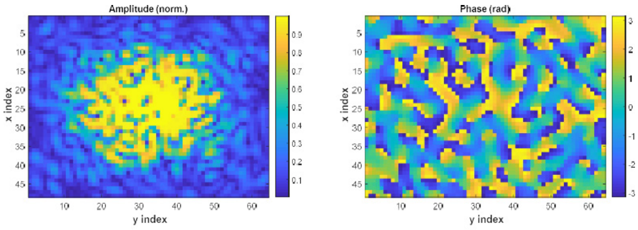

(a) (b)

Fig. 9 The synthesized circular footprint: (a) Amplitude excitations; (b) Phase excitations

degrees of freedom for synthesizing properly such arbitrary complex shape. The shape of the targeted Iraq-Land footprint is shown in Fig. 10 (a), while the shape of the synthesized Iraq-Land footprint is shown in Fig. 10 (b).

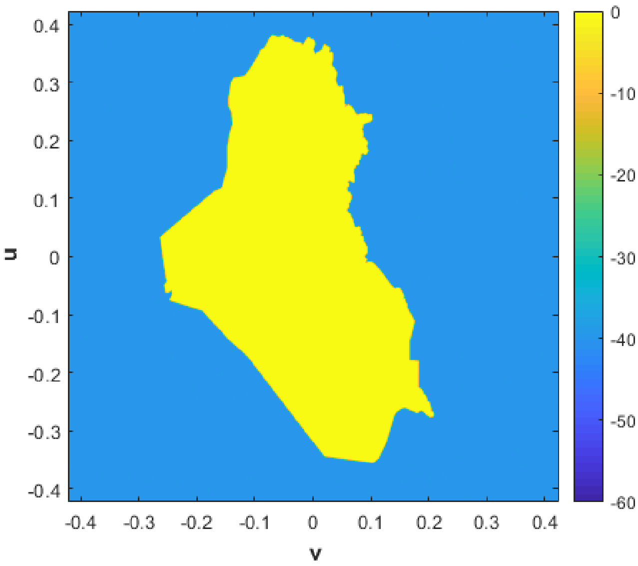

(a)

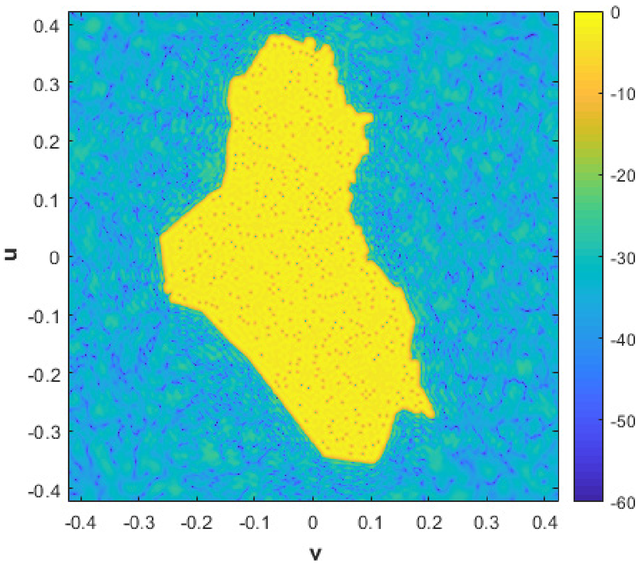

(b)

Fig. 10 The results of Iraq outline footprint: (a) Desired shape; (b) Synthesized shape

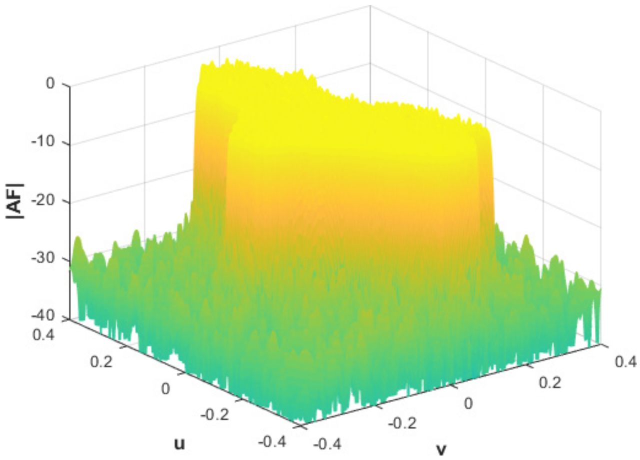

Fig. 11 The 3D plot of the synthesized Iraq outline footprint radiation pattern

The three-dimension plot of the obtained far-field radiation pattern is shown in Fig. 11. From Fig. 11, it can be seen that the required far-field radiation footprint has been precisely met and the peak sidelobe level of the radiated power outside the footprint's boundary has been reduced to more than −27.8 dB. The corresponding amplitude and phase excitations of the designed planar array are shown in Fig. 12. From Fig. 12, it can be seen that the normalized elements excitations are distributed between $0 < w_{n,m} \leq 1$ where the majority of edge elements have a smaller magnitudes than the central elements.

This means that there are a large number of the edge elements that have weak magnitudes less than a certain threshold value. These weak elements may have relatively small contribution to the resulting array pattern and they are still active elements that consume RF attenuators.

Finally, the thinning process according to Eq. (6) is applied to the Iraq-Land footprint synthesis process to reduce the number of active array elements as well as to improve the DRR. For threshold = 0.05, the percentage of weak elements removal is 18.39%, while the DRR = 20. For another case of threshold = 0.1, the percentage of weak elements removal is 21.56%, the DRR = 10. Fig. 13 shows the 2D and 3D of the synthesized Iraq-Land footprint with thinning weak elements at high value of threshold = 0.05. The DRR is only 2. The normalized element amplitude and phase excitations are shown in Fig. 14. Although there is an increase in the sidelobe level of the synthesized footprint due to the removal of large number of elements about 75.65%, the Iraq-Land footprint shape is still clear and acceptable with peak sidelobe level of −17.6 dB. Table 1 summarizes the performance measures of the iterative FFT method under various thinning percentage. It can be seen that when increasing the thinning

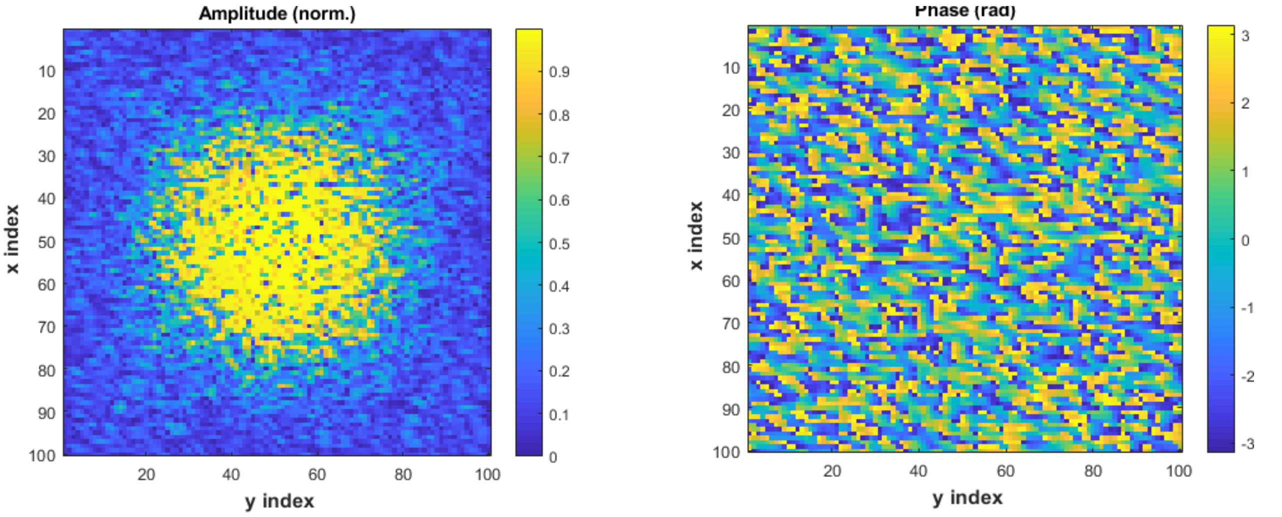

(a) (b)

Fig. 12 The synthesized Iraq outline footprint: (a) Amplitude excitations; (b) Phase excitations

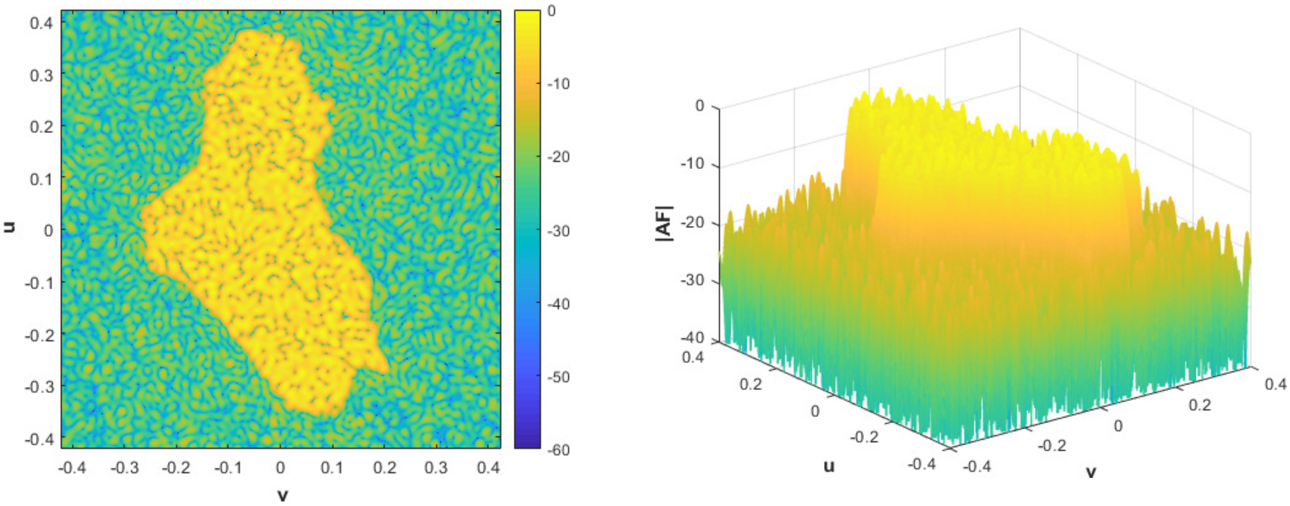

(a) (b)

Fig. 13 The Iraq outline footprint radiation patterns: (a) 2D pattern; (b) 3D pattern

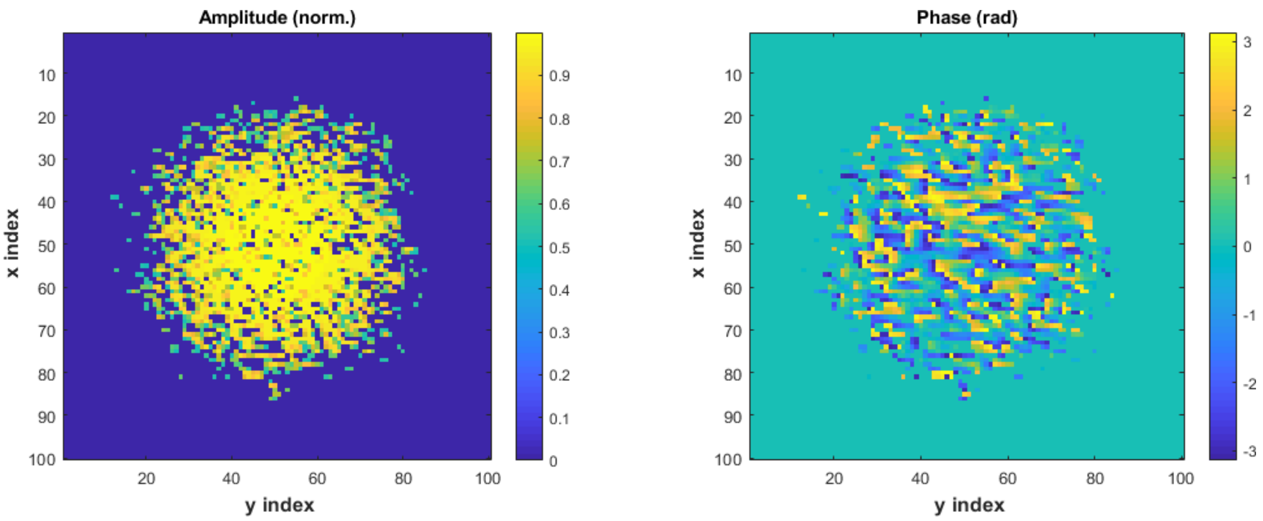

(a) (b)

Fig. 14 The synthesized Iraq outline footprint with thinned elements at threshold value of 0.5: (a) Amplitude excitations; (b) Phase excitations

Table 1 Performance measures under various thinning percentage

The method	Thinning percentage	DRR	SLL	Mainbeam ripples
Standard IFFT without thinning	0%	100	−30 dB	−0.5 dB
IFFT with threshold value of 0.05	18.39%	20	−25 dB	−1.8 dB
IFFT with threshold value of 0.1	21.56%	10	−20 dB	−2.3 dB
IFFT with threshold value of 0.5	75.65%	2	−17.6 dB	−6.0 dB

percentage (i.e., increasing the percentage of the weak elements removal) the dynamic range ration (DRR) will be improved while the sidelobe level and the ripple magnitudes in the main beam region will be increased.

5 Conclusions

To achieve a precise coverage on the targeted region, the array radiation patterns should be synthesized according to these coverage boundaries. The iterative FFT method, which is characterized as a fast convergence speed algorithm compared to all other optimization algorithms, has been proved to be one of the best methods to accurately target arbitrary footprints. Three simple footprint shapes such as triangular, square, circular, and another one which is a quite complex shape of Iraq-Land were synthesized. All of these targeted footprints have been effectively generated by controlling simultaneously the element excitation amplitudes and phases of the planar array. In all of the synthesized footprint patterns, the peak sidelobe level was below −20 dB which is quite acceptable. Moreover, a thinning process for reducing the array cost and complexity was introduced to remove the weak elements that have a small amplitude and negligible effect on the footprint's pattern formulation. This thinning strategy also helps to improve the dynamic range ratio.

References

[1] Cai, M., Li, W., Shi, X., Zhang, Q., Liu, H., Li, Y., Wan, J., Gao, S. "Design and Simulations of a Novel Ka-Band Isoflux Scanning Phased Array Antenna for GEO Satellites", IEEE Antennas and Wireless Propagation Letters, 23(2), pp. 738–742, 2024. https://doi.org/10.1109/LAWP.2023.3335370

[2] Mohammed, J. R. "Low Complexity Adaptive Noise Canceller for Mobile Phones Based Remote Health Monitoring", International Journal of Electrical and Computer Engineering (IJECE), 4(3), pp. 422–432, 2014. https://doi.org/10.11591/ijece.v4i3.5534

[3] Mohammed, J. R., Singh, G. "An Efficient RLS Algorithm For Output-Error Adaptive IIR Filtering And Its Application To Acoustic Echo Cancellation", In: 2007 IEEE Symposium on Computational Intelligence in Image and Signal Processing, Honolulu, HI, USA, 2007, pp. 139–145. ISBN 1-4244-0707-9 https://doi.org/10.1109/CIISP.2007.369307

[4] Yang, X., Liu, X. "Design of a Wide-Beam Microstrip Array Antenna for Automotive Radar Application", IEEE Access, 9, pp. 142340–142347, 2021. https://doi.org/10.1109/ACCESS.2021.3119756

[5] Lin, J., Cao, Y., Che, W., Xue, Q. "Wide-Angle and Wideband Millimeter-Wave Beam-Scanning Array Using Multimode Shorted Patch Antenna Elements for Unmanned Aerial Vehicle Communication", IEEE Transactions on Vehicular Technology, 74(1), pp. 537–545, 2025. https://doi.org/10.1109/TVT.2024.3462456

[6] Ares, F., Fondevila-Gómez, J., Franceschetti, G., Moreno-Piquero, E., Rodríguez-González, J. A. "Synthesis of Very Large Planar Arrays for Prescribed Footprint Illumination", IEEE Transactions on Antennas and Propagation, 56(2), pp. 584–589, 2008. https://doi.org/10.1109/TAP.2007.915472

[7] Morabito, A. F., Laganà, A. R., Sorbello, G., Isernia, T. "Mask-constrained power synthesis of maximally sparse linear arrays through a compressive-sensing-driven strategy", Journal of Electromagnetic Waves and Applications, 29(10), pp. 1384–1396, 2015. https://doi.org/10.1080/09205071.2015.1046561

[8] Mohammed, J. R. "Rectangular Grid Antennas with Various Boundary Square-Rings Array", Progress In Electromagnetics Research Letters, 96, pp. 27–36, 2021. https://doi.org/10.2528/PIERL20112402

[9] Battaglia, G. M., Morabito, A. F., Sorbello, G., Isernia, T. "Mask-Constrained Power Synthesis of Large and Arbitrary Arraysas a Few-Samples Global Optimization", Progress In Electromagnetics Research C, 98, pp. 69–81, 2020. https://doi.org/10.2528/PIERC19082904

[10] Mohammed, J. R. "Simplified Rectangular Planar Array with Circular Boundary for Side lobe Suppression", Progress In Electromagnetics Research M, 97, pp. 57–68, 2020. https://doi.org/10.2528/PIERM20062906

[11] Battaglia, G. M., Bellizzi, G. G., Morabito, A. F., Sorbello, G., Isernia, T. "A general effective approach to the synthesis of shaped beams for arbitrary fixed-geometry arrays", Journal of Electromagnetic Waves and Applications, 33(18), pp. 2404–2422, 2019. https://doi.org/10.1080/09205071.2019.1683472

[12] Mohammed, J. R. "An optimum side-lobe reduction method with weight perturbation", Journal of Computational Electronics, 18(2), pp. 705–711, 2019. https://doi.org/10.1007/s10825-019-01323-5

[13] Pour, M., Mitha, T. H., Brothers, E. C. "A Combined Electronic Position- and Partial Amplitude-Control Synthesis Technique for Sidelobe Reductions in Linear Array Antennas", IEEE Transactions on Microwave Theory and Techniques, 71(12), pp. 5074–5081, 2023.
https://doi.org/10.1109/TMTT.2023.3288634

[14] Mohammed, J. R. "Obtaining wide steered nulls in linear array patterns by optimizing the locations of two edge elements", AEU - International Journal of Electronics and Communications, 101, pp. 145–151, 2019.
https://doi.org/10.1016/j.aeue.2019.02.004

[15] Haupt, R. L. "Antenna Arrays: A Computational Approach", John Wiley & Sons, Inc., 2010. ISBN 9780470407752
https://doi.org/10.1002/9780470937464

[16] Sayidmarie, K. H., Mohammed, J. R. "Performance of a Wide Angle and Wide Band Nulling Method for Phased Arrays", Progress in Electromagnetics Research M, 33, pp. 239–249, 2013.
https://doi.org/10.2528/PIERM13100603

[17] Boeringer, W. D., Werner, D. H. "Efficiency-Constrained Particle Swarm Optimization of a Modified Bernstein Polynomial for Conformal Array Excitation Amplitude Synthesis", IEEE Transactions on Antennas and Propagation, 53(8), pp. 2662–2673, 2005.
https://doi.org/10.1109/TAP.2005.851783

[18] Mohammed, J. R. "A New Technique for Obtaining Wide-Angular Nulling in the Sum and Difference Patterns of Monopulse Antenna", IEEE Antennas and Wireless Propagation Letters, 11, pp. 1245–1248, 2012.
https://doi.org/10.1109/LAWP.2012.2224086

[19] Li, W.-Z., Jiao, Y.-C., Zhang, Y.-X., Zhang, L. "Synthesis of Sum-and-Difference Patterns for Radome-Enclosed Linear Arrays With Common Weights Using Convex Optimization", IEEE Antennas and Wireless Propagation Letters, 24(3), pp. 607–611, 2025.
https://doi.org/10.1109/LAWP.2024.3509618

[20] Mohammed, J. R., Thaher, R. H., Abdulqader, A. J. "Linear and Planar Array Pattern Nulling via Compressed Sensing", Journal of Telecommunications and Information Technology, 85(3), pp. 50–55, 2021.
https://doi.org/10.26636/jtit.2021.152921

[21] Yang, X., Yang, D., Zhao, Y., Pan, J., Chen, Y. "Synthesis of Linear Sparse Array Using DNN-Based Machine-Learning Method", IEEE Transactions on Antennas and Propagation, 71(8), pp. 6513–6522, 2023.
https://doi.org/10.1109/TAP.2023.3278878

[22] Rodriguez, J. A., Botha, E., Ares, F. "Extension of the Orchard-Elliott synthesis method to pure-real nonsymmetrical-shaped patterns", IEEE Transactions on Antennas and Propagation, 45(8), pp. 1317–1318, 1997.
https://doi.org/10.1109/8.611254

[23] Li, J.-Y., Qi, Y.-X., Zhou, S.-G. "Shaped Beam Synthesis Based on Superposition Principle and Taylor Method", IEEE Transactions on Antennas and Propagation, 65(11), pp. 6157–6160, 2017.

[24] Mohammed, J. R. "Phased array antenna with ultra-low sidelobes", Electronics Letters, 49(17), pp. 1055–1056, 2013.
https://doi.org/10.1049/el.2013.1642

[25] Wang, X.-K., Jiao, Y.-C., Tan, Y. Y. "Gradual Thinning Synthesis for Linear Array Based on Iterative Fourier Techniques", Progress In Electromagnetics Research, 123, pp. 299–320, 2012.
https://doi.org/10.2528/PIER11100903

[26] Mohammed, J. R., Abdulqader, A. J. "Array Pattern Restoration under Defective Elements", Progress in Electromagnetics Research C, 123, pp. 17–26, 2022.
https://doi.org/10.2528/PIERC22061101

[27] Mohammed, J. R. "Design of Printed Yagi Antenna with Additional Driven Element for WLAN Applications" Progress in Electromagnetics Research C, 37, pp. 67–81, 2013.
https://doi.org/10.2528/PIERC12121201